Research Square

Preprints are preliminary reports that have not undergone peer review.
They should not be considered conclusive, used to inform clinical practice,
or referenced by the media as validated information.

Identifying Lipid Metabolites Influenced by Brefeldin A in Hepatocellular Carcinoma Cells Using Targeted Lipidomics

Yifan Zhao
Shanxi Medical University
Jinzhi Song
Shanxi Medical University
Ying Yang
Shanxi Medical University
Mengyi Duan
Shanxi Medical University
Yang Chen
Shanxi Medical University
Minfei Hou
Shanxi Medical University
Yuchao Hao
Shanxi Medical University
Xiaotong Ji
Shanxi Medical University
Jianying Bai
jybai66@sxmu.edu.cn

Shanxi Medical University

Research Article

Keywords: Brefeldin A, lipidomics, hepatocellular carcinoma, sphingolipid metabolism

Posted Date: September 10th, 2026

DOI: https://doi.org/10.21203/rs.3.rs-10466838/v1

License: This work is licensed under a Creative Commons Attribution 4.0 International License.
Read Full License

Additional Declarations:
No competing interests reported.

Tables are available in the Supplementary Files section.

Identifying Lipid Metabolites Influenced by Brefeldin A in Hepatocellular Carcinoma Cells Using Targeted Lipidomics

Yifan Zhao [a], Jinzhi Song[a], Ying Yang[a],Mengyi Duan[a], Chen Yang[a],Minfei Hou[a], Yuchao Hao[a],Xiaotong Jl[a,b,c,d], Jianying Bai [a,b,c,d]

[a] Department of Environmental Health, School of Public Health, Shanxi Medical University, Taiyuan, Shanxi 030001, China

[b] MOE Key Laboratory of Coal Environmental Pathogenicity and Prevention, Taiyuan, Shanxi 030001, China

[c] Center for Ecological Public Health Security of Yellow River Basin, Shanxi Medical University, Taiyuan, Shanxi 030001, China

[d]Shanxi Key Laboratory of Environmental Pollution Pathogenicity and Prevention

[*] **Corresponding author:** Jianying Bai (jybai66@sxmu.edu.cn)

Abstract

Purpose Brefeldin A (BFA) is known to induce endoplasmic reticulum stress and apoptosis in HepG2 cells, a human hepatocellular carcinoma (HCC) cell line, but its impact on cancer-associated lipid metabolic reprogramming remains unclear. The occurrence and

progression of HCC are often accompanied by lipid metabolic abnormalities. This study aimed to systematically profile BFA-induced lipid alterations using targeted lipidomics and to characterize the lipid metabolic alterations to counteract the lipid metabolic reprogramming in HCC cells following BFA treatment.

Methods Targeted lipidomics based on UHPLC-QTRAP MS was applied to HepG2 cells treated with 0.25 mg/L BFA for 24 h (n = 6 per group). Lipids with VIP > 1.0 from OPLS-DA and FDR < 0.05 (Benjamini–Hochberg corrected) were considered significantly altered. Lipid contents were normalized to total protein (pg/10^6 cells).

Results A total of 481 lipid species were significantly altered across 21 classes. Concentrations of lysophosphatidylcholine (LPC), hexosylceramides (Hex1Cer), lactosylceramides (Hex2Cer), cholesterol esters (ChE), and triglycerides (TG) were markedly elevated, while FA(24:0) was significantly decreased.

Conclusion BFA can significantly increase the contents of Hex1Cer, Hex2Cer and LPC in HCC,which may contribute to its anticancer activity. This lipid-centric dataset provides a resource for understanding BFA's cellular effects and identifies candidate lipid species for further investigation in HCC.

KEYWORDS: Brefeldin A; lipidomics; hepatocellular carcinoma; sphingolipid metabolism

Globally, liver cancer is one of the most common fatal malignancies. In the United States, it ranks fifth in cancer mortality[1], while in China, both its incidence and mortality rates rank third among all cancers[2]. Given the poor prognosis of liver cancer patients, exploring novel therapeutic strategies is necessary and urgent. Brefeldin A (BFA), a protein transport inhibitor, is a macrolide antibiotic synthesized by fungi and is a metabolic product of various strains including Penicillium, Penicillium chrysogenum, and Aspergillus clavatus. BFA primarily inhibits ARF1-dependent COPI coat formation[3], leading to the disassembly of the Golgi apparatus and its retrograde fusion into the endoplasmic reticulum[4]. This blocks protein transport from the endoplasmic reticulum

to the Golgi, thereby triggering endoplasmic reticulum stress and inducing apoptosis in hepatocellular carcinoma (HCC) cells[5].

The rapid proliferation of tumor cells is inseparable from their metabolic reprogramming, among which lipid metabolic reprogramming not only meets cellular energy demands but also provides necessary materials for proliferation and signaling molecules for various oncogenic pathways[6]. In HCC, the occurrence and progression are closely associated with dysregulated lipid metabolism, characterized by enhanced de novo fatty acid and cholesterol synthesis, as well as fatty acid oxidation[7]. Moreover, dysregulation of specific lysophospholipid species, including saturated lysophosphatidylcholine (LPC) and lysophosphatidylethanolamine (LPE) species, has been implicated in HCC pathogenesis and progression[8].

Lipidomics has emerged as a powerful tool for dissecting these metabolic alterations in HCC and other liver diseases[9]. Whether BFA can counteract the lipid metabolic abnormalities in HepG2 cells remains unclear. In this study, targeted lipidomics was used to systematically profile lipid metabolite alterations in BFA-treated HepG2 cells, aiming to provide a comprehensive lipid-centric characterization of BFA-induced metabolic changes that may contribute to understanding its cellular effects in HCC.

Statistical Analysis of Lipid Metabolites from BFA Treated Groups

To visualize the overall metabolic differences between groups and identify the lipid species most responsible for this discrimination, we performed partial least squares-discriminant analysis (PLS-DA). The PLS-DA score plots[10] (Figure 1A) showed a clear separation between the BFA-treated and vehicle control groups, with tight clustering of samples within each group demonstrating high analytical reproducibility. The model's goodness of fit ($R^2Y = 0.99$) and predictive ability ($Q^2 = 0.97$) were excellent. A permutation test with 200 random permutations (Figure 1B) was performed to validate the model. The negative intercept of the Q^2 regression line with the Y-axis indicates that the model is not overfitting[11]. Taken together, these multivariate analyses demonstrate that BFA treatment causes significant and reliable lipid metabolic reprogramming in HepG2 cel

ls.

To further identify the specific lipid molecules responsible for the separation observed in th e multivariate models, univariate statistical analysis was performed. The differential abundance o f all detected lipids between BFA-treated and vehicle control groups is visualized in the volcano plot (Figure 2). Lipid species with a fold change (FC) > 1.5 or < 0.67 and a false discovery rate (FDR) < 0.05 (Benjamini-Hochberg adjusted) were considered statistically significant. Based on these criteria, a total of 481 lipid species were identified as significantly altered in response to B FA treatment. Among these, a substantial number of lipids show both significant adjusted p-value s and large fold changes, clustering in the upper-right and upper-left quadrants of the plot. These significantly altered lipid species were selected for further investigation as candidate markers of BFA-induced metabolic perturbation.

To further explore the overall pattern of BFA-induced lipid changes, the significantly altered lipids were categorized and visualized at the lipid class level. The bubble plot (Figure 3) provide s an overview of these changes, where significantly altered lipid species (VIP > 1.0 and FDR < 0. 05) are grouped by their class membership[12]. The position of bubbles along the x-axis indicates t he percentage difference in abundance between BFA and control groups, while bubble size corres ponds to the statistical significance ($-\log_{10}$(p-value)).

Identification of Lipid Metabolites by UHPLC-QTRAP MS

The lipids influenced by BFA treatment are classified into 21 major classes belonging to fo ur principal categories: phospholipids, sphingolipids, neutral lipids, and other lipids. The detailed classification comprised: phospholipids—lysophosphatidylethanolamine (LPE), lysophosphatid ylcholine (LPC), phosphatidylglycerol (PG), phosphatidylinositol (PI), phosphatidylserine (PS), phosphatidylethanolamine (PE), plasmenyl phosphatidylethanolamine (PE-P), plasmanyl phosph atidylethanolamine (PE-O), phosphatidylcholine (PC), phosphatidic acid (PA), and lysophosphati dylglycerol (LPG); sphingolipids—ceramide (Cer), dihydroceramide (DHCer), hexosylceramide (Hex1Cer), lactosylceramide (Hex2Cer), and sphingomyelin (SM); neutral lipids—monoacylgly cerol (MG), diacylglycerol (DG), triacylglycerol (TG), and cholesterol ester (ChE); and other lipi

ds—fatty acid (FA). Statistical analysis revealed that four lipid classes, including Hex2Cer, ChE, LPC, and TG, demonstrate a general increasing trend following BFA administration. In addition, numerous other lipid species exhibiting significant alterations in response to BFA treatment were considered candidate markers of BFA-induced metabolic perturbation. The absolute contents of all 21 lipid classes are listed in Table S1 (Supporting Information).

Significant Changes of Lipid Metabolites in BFA-Treated Groups

Using targeted lipidomics based on UHPLC-QTRAP MS, we investigated the changes in lip id metabolites after BFA treatment. The results showed that over 1,000 lipid species were identifi ed and categorized into four major categories: phospholipids, sphingolipids, neutral lipids, and ot hers. Differential lipids were identified based on a combination of multivariate and univariate an alysis. As shown in Figure 4, significant differences were observed in several major classes. Spec ifically, the levels of LPC, Hex2Cer, and ChE were significantly increased compared to the vehic le control group. The neutral lipid TG was also notably elevated. Furthermore, changes in the lev els of specific lipid species were assessed as representative markers of BFA-induced lipid metabo lic changes which may contribute to its antitumer propertity. These included LPC(16:0), LPC(17: 0), LPC(18:0), and LPC(20:0) (Figure 5); Hex1Cer(d18:1/16:0), Hex1Cer(d18:1/24:0), Hex1Cer (d18:1/24:1), and Hex1Cer(d18:1/26:1), as well as Hex2Cer(d18:1/16:0), Hex2Cer(d18:1/22:0), Hex2Cer(d18:1/24:0), and Hex2Cer(d18:1/24:1) (Figure 5); FA(24:0) (Figure 5); and ChE(20:3), ChE(20:4), ChE(18:3), and ChE(22:6), as well as TG(48:0)-FA16:0, TG(52:2)-FA16:0, TG(54: 4)-FA20:4, and TG(56:6)-FA22:6 (Figure 5).

Discussion

In this study, targeted lipidomics revealed extensive lipid remodeling in HepG2 cells followi ng BFA treatment, with 481 lipid species significantly altered across 21 classes. Notably, the acc umulation of LPC, Hex1Cer, Hex2Cer, ChE, and TG, along with a significant decrease in FA(24: 0), points to a coordinated alteration of phospholipid, sphingolipid, and neutral lipid metabolism. In the following sections, we discuss these class-level and species-level changes in the context o

f known lipid biology and BFA's established cellular effects, while acknowledging that the curre nt dataset is descriptive and does not directly establish causal relationships.

The contents of LPC (16:0), LPC (17:0), LPC (18:0), and LPC (20:0) were significantly hig her in the BFA-treated group compared to the vehicle control. The marked rise in LPC implies a disturbance in phospholipid metabolism induced by BFA. As a product of phosphatidylcholine h ydrolysis by phospholipase A2 (PLA2), the accumulation of LPC may reflect enhanced degradati on of membrane phospholipids[13]. LPC is a cytotoxic lipid molecule that can promote cellular stre ss and apoptosis through multiple mechanisms. It can activate G protein-coupled receptors (GPC Rs), such as the G2A receptor, thereby triggering pro-apoptotic signaling, which is beneficial fo r cancer treatment[14]. Furthermore, LPC can induce a burst of reactive oxygen species (ROS), exa cerbating oxidative damage[15]. Studies have also shown that LPC can directly activate the c-Jun N -terminal kinase (JNK) pathway, which plays a crucial role in regulating cellular stress and apopt osis[16]. Additionally, LPC can intensify the unfolded protein response (UPR) via the IRE-1α/XBP-1s signaling axis[17], leading to the upregulation of pro-apoptotic proteins like CHOP, which syner gizes with the JNK pathway to promote apoptosis[18]. LPC molecules can also activate protein kina se C (PKC) through GPCRs, thereby participating in the regulation of apoptosis. Notably, LPC(1 6:0) plays a significant role in normal cellular activity; however, under pathological conditions, it has been associated with disruption of the phospholipid bilayer, induction of inflammation, and a ctivation of inflammatory transcription factors such as NF-κB. Collectively, these observations su ggest that the BFA-induced LPC accumulation may contribute to pro-apoptotic effects in HepG2 cells.

Following BFA treatment, significant alterations in sphingolipid metabolism were observed. We noted a marked increase in the levels of several Hex1Cer and Hex2Cer molecular species in the BFA-treated group, specifically including Hex1Cer(d18:1/16:0), Hex1Cer(d18:1/24:0), Hex1 Cer(d18:1/24:1), Hex1Cer(d18:1/26:1), Hex2Cer(d18:1/16:0), Hex2Cer(d18:1/22:0), Hex2Cer(d 18:1/24:0), and Hex2Cer(d18:1/24:1). This outcome may be closely linked to BFA-induced disru ption of Golgi apparatus function.

Existing studies confirm that BFA can induce the merger of the cis-Golgi membrane with th e endoplasmic reticulum (ER), a process that may alter key enzymes involved in sphingolipid sy nthesis[19]. BFA has been shown to enhance the glucosylation of ceramide [20]and can induce glycos ylation of Ceramide Synthase 6 (CerS6), leading to the accumulation of endogenous C16:0-cera mide[21]. Therefore, it is plausible that BFA may directly or indirectly promote the ceramide gluco sylation reaction catalyzed by Glucosylceramide Synthase (GCS), thereby driving the synthesis a nd accumulation of Hex1Cer and its downstream products. Furthermore, BFA has also been class ified as a regulator of ganglioside GM3 synthase (ST3GAL5, a downstream enzyme for the furth er metabolism of Hex1Cer). Similarly, Hayashi et al. also reported that BFA treatment significan tly elevated GM3 levels in human colon cancer cells (HCT 116), the synthetic precursors of whic h include Hex1Cer[22].

The extra accumulation of Hex1Cer and Hex2Cer is closely associated with ER stress and mitochondrial dysfunction[23]. Notably, BFA itself has been proven to cause protein accumulation within the ER, trigger ER stress, and induce apoptosis. It is plausible that the observed sphingoli pid accumulation in this study may act synergistically with this process. On one hand, the accum ulation of these sphingolipids can exacerbate ER stress, leading to the upregulation of pro-apopto tic proteins like CHOP[23]. This, in turn, may inhibit anti-apoptotic BCL-2 family proteins and acti vate the Caspase-8/-10 cascade via the death receptor pathway. On the other hand, excessive Hex 2Cer, which has a binding affinity for cardiolipin three times greater than Hex1Cer, has been rep orted to inhibit mitochondrial complex IV activity. This may lead to increased mitochondrial rea ctive oxygen species (ROS) production[24], alterations in membrane potential, and ultimately, activ ation of Caspase-3 to induce apoptosis[25].

It is important to note that the biological functions of ceramides and their derivatives vary d epending on their fatty acid chain length. For instance, C16:0-ceramide and its derivatives Hex1 Cer/Hex2Cer, primarily synthesized by Ceramide Synthase 5/6 (CerS5/6), exhibit well-defined p ro-apoptotic properties[26]. In contrast, very long-chain sphingolipids such as C22:0-C24:1 are mai nly catalyzed by Ceramide Synthase 2 (CerS2) and are primarily involved in maintaining cell me

mbrane stability[27]. The widespread increase in sphingolipids of various chain lengths induced by BFA may simultaneously disrupt the balance between pro-apoptotic signaling and anti-apoptotic signaling. And also disrupt mitochondrial membrane stability.

Furthermore, against the backdrop of a general increase in multiple lipid categories, this stu dy detected a significant decrease in the content of the very long-chain saturated fatty acid FA(2 4:0) (lignoceric acid). FA(24:0) is a core precursor for the synthesis of C24-chain ceramide, used in the generation of Hex1Cer and Hex2Cer. Research indicates that the biosynthetic flux of very l ong-chain ceramides (e.g., C24:0) is significantly higher than that of long-chain ceramides, leadi ng to their faster metabolic conversion into sphingomyelin and hexosylceramides[28]. Therefore, th e decrease in FA(24:0) suggests that BFA may heavily mobilize this exogenous precursor and dir ect it toward the sphingolipid synthesis pathway.

Following BFA treatment, a substantial accumulation of neutral lipids was observed in Hep G2 cells, specifically manifested as significant increases in the levels of ChE and TG (pg/10^6 cell s). The contents of multiple ChE molecular species — including ChE(20:3), ChE(20:4), ChE(18: 3), and ChE(22:6) — as well as several specific TG species, such as TG(48:0)-FA16:0, TG(52: 2)-FA16:0, TG(54:4)-FA20:4, and TG(56:6)-FA22:6, were markedly higher in the BFA-treated g roup compared to the vehicle control.

The significant elevation of intracellular TG and ChE levels induced by BFA in HepG2 cells may be attributed to the following reasons. BFA binds to guanine nucleotide exchange factors (GEFs), preventing ARF activation and leading to COPI coat disassembly and subsequent inhibit ion of vesicular transport[4]. In hepatocytes, triglycerides (TG) are primarily exported in the form of very low-density lipoprotein (VLDL) via vesicular trafficking. Thus, BFA-induced impairmen t of vesicular transport may suppress VLDL secretion, resulting in the accumulation of TG withi n the ER and the subsequent formation of lipid droplets[29]. Concurrently, ER dysfunction may pro mpt cells to upregulate acyl-CoA:cholesterol acyltransferase (ACAT) activity, esterifying free ch olesterol into ChE[30]. Furthermore, transport impairments might lead to the abnormal mobilizatio n of some membrane lipids for TG synthesis. These aberrant metabolic processes further exacerb

ate the intracellular accumulation of lipids[29].

At the same time, high levels of ChE may physically alter ER membrane fluidity. The resultant imbalance in ER homeostasis hinders COPI vesicle transport, leading to the accumulation of misfolded proteins and impairing the unfolded protein response (UPR) capacity[31], ultimately inducing cellular stress or even death. TG metabolic imbalance is closely associated with elevated intracellular oxidative stress[32]. The lipolysis of stored TG may generate excessive fatty acids, overloading mitochondrial β-oxidation and causing dysfunction of the electron transport chain, thereby triggering excessive production of reactive oxygen species (ROS). Prolonged redox imbalance can further damage organelle function and interfere with quality control systems such as autophagy[33].

In summary, the present lipidomics study reveals that BFA extensively remodels the lipid landscape of HepG2 cells, with significant accumulation of LPC, Hex1Cer, Hex2Cer, ChE, and TG, alongside a decrease in FA(24:0). These alterations point to a coordinated perturbation of phospholipid, sphingolipid, and neutral lipid metabolism. The observed lipid changes are consistent with known pro-apoptotic and stress-inducing functions of these lipid classes, and may synergize with BFA's established ER stress-inducing activity to contribute to its anti-proliferative effects in HCC cells. However, we acknowledge that the present study is descriptive and limited to a single cell line and treatment condition; direct causal relationships between the observed lipid changes and apoptosis or other functional outcomes have not been established. Future studies incorporating functional assays (e.g., lipid supplementation or synthesis inhibition) and additional cell lines (including normal hepatocytes) are warranted to validate the biological significance of these lipidomic alterations. Nevertheless, this work provides a comprehensive lipid-centric dataset that may serve as a resource for generating hypotheses regarding BFA's metabolic effects and for identifying candidate lipid species for further investigation in HCC.

Figure 1. Multivariate analysis of lipidomic profiles from BFA-treated and vehicle control groups. **(A)** Partial least squares-discriminant analysis (PLS-DA) score plot showing clear separation between BFA-treated (green squares, n = 6) and vehicle control (blue circles, n = 6) groups. The ellipse represents the 95% confidence region (Hotelling's T^2). **(B)** Permutation test (200 permutations) for validating the PLS-DA model, showing goodness of fit (R^2Y, green boxes) and predictive ability (Q^2, blue boxes). The original model (far right) has $R^2 = 0.99$ and $Q^2 = 0.97$, indicating a robust and non-overfit model.

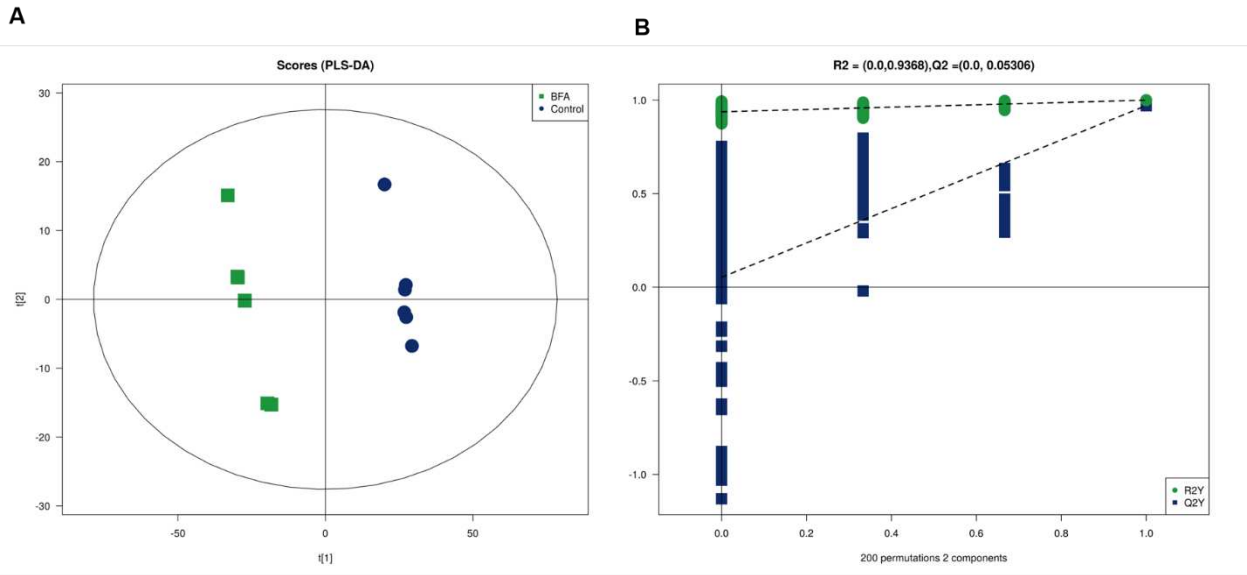


Figure 2. Volcano plot visualizing lipid metabolites with significant alterations upon BFA treatment. Volcano plots were obtained from all identified molecules from the positive and negative modes. Red points indicate lipid species with significantly different abundances after BFA treatment (FDR < 0.05, $|\mathbf{log_2FC}| > \mathbf{0.585}$, corresponding to fold change > 1.5 or < 0.67). Black points indicate compounds not significantly influenced by BFA treatment. Lipid species to the right of the right threshold increased with BFA treatment, while those to the left of the left threshold decreased. FC, fold change.

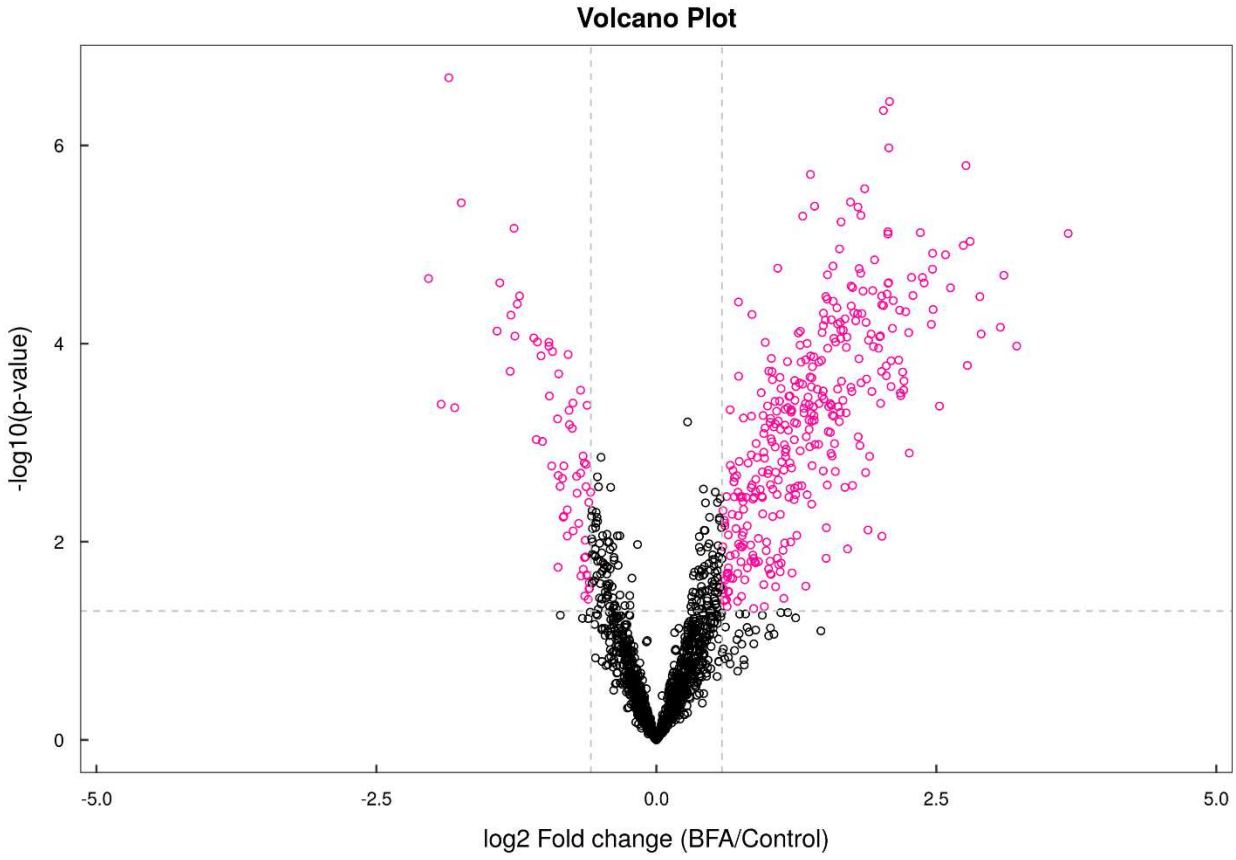


Figure 3. Bubble chart showing the relative content differences of different lipid categories. Significantly altered lipid species (VIP > 1.0 and FDR < 0.05) are grouped by their class membership (y-axis). The x-axis represents the percentage difference. A negative value indicates that the lipid has a higher relative content in the vehicle control group, while a positive value indicates a higher relative content in the BFA-treated group. The size of each bubble corresponds to the statistical significance ($-\log_{10}$(adjusted p-value)) of the change.

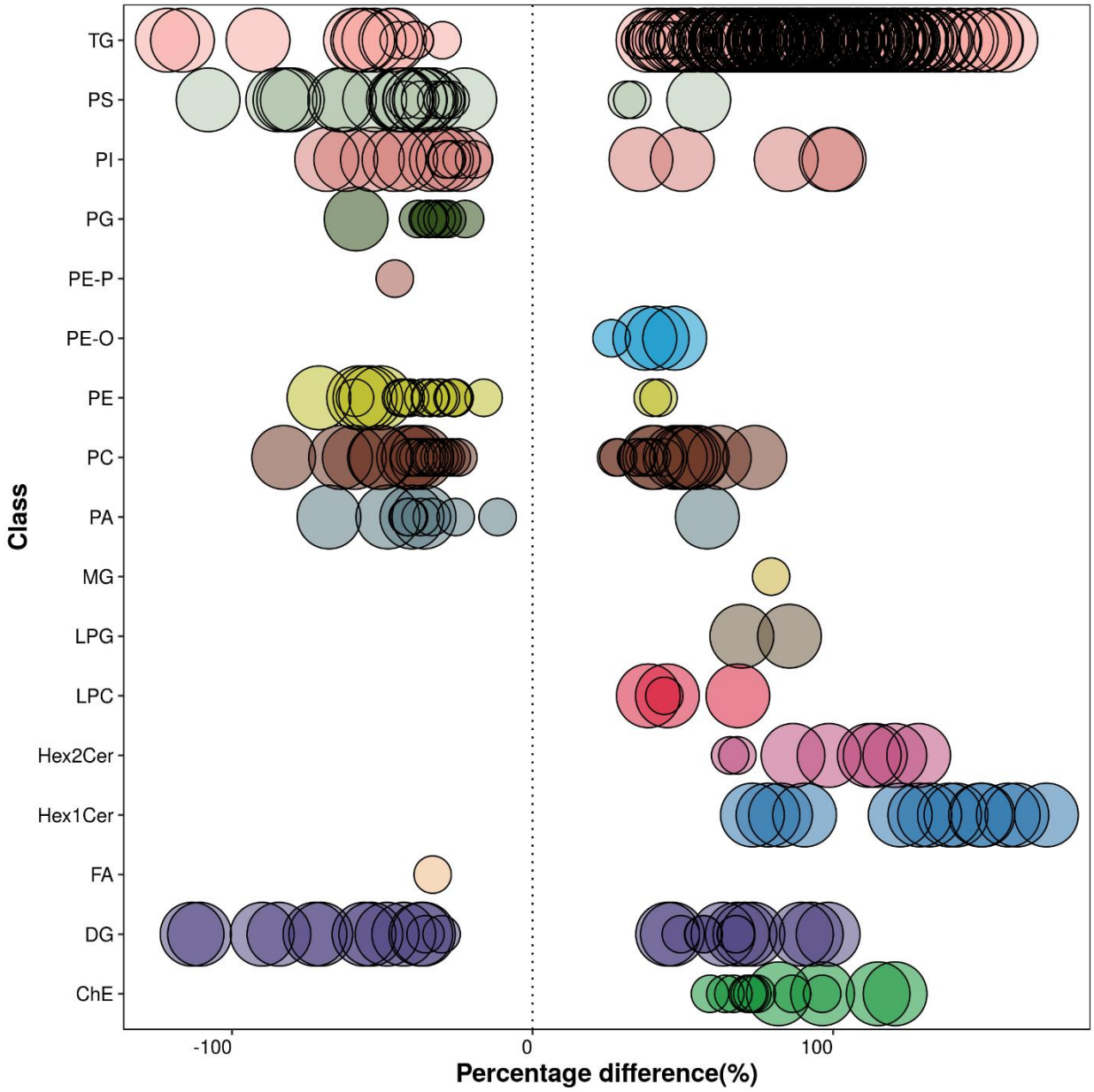


Figure 4. Bar charts showing the absolute contents (pg/10^6 cells) of 21 lipid classes detected after BFA treatment. **A** Phospholipids: PI, PC, PG, PS, PE, and PE-P. **B** Phospholipids continued: LPC, LPE, PE-O, and PE-P. **C** Sphingolipids: Cer, SM, DHCer, Hex1Cer, and Hex2Cer. **D** Other lipids: FA, MG, PA, and LPG. Data are presented as mean ± SD (n = 6). Blue bars represent vehicle control groups, and red bars represent BFA-treated groups. Statistical comparisons were performed using Student's t-test with FDR correction. *$p < 0.05$, **$p < 0.01$, ***$p < 0.001$ vs

vehicle control.

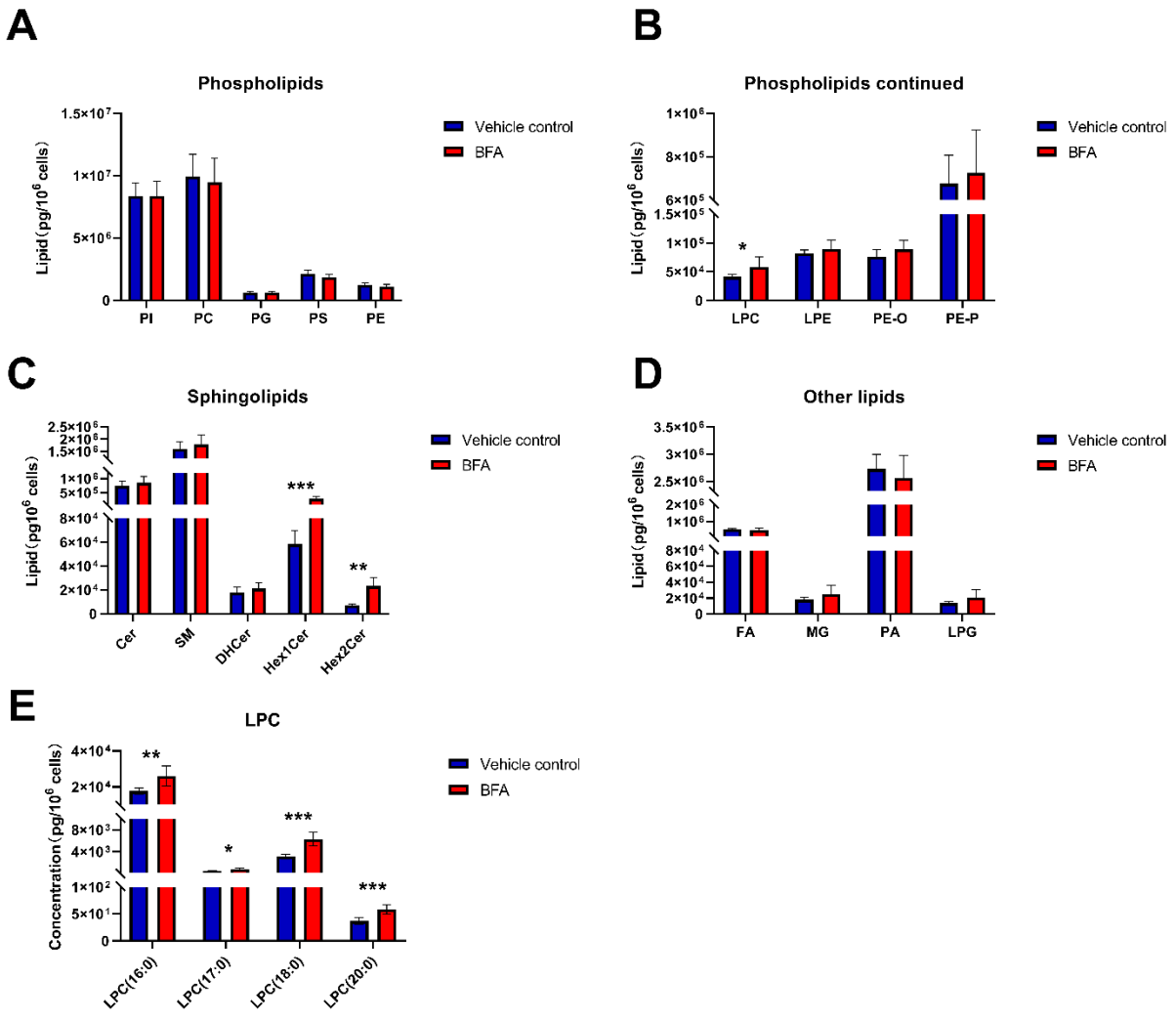
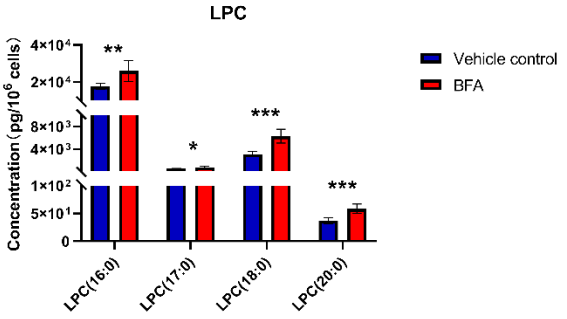
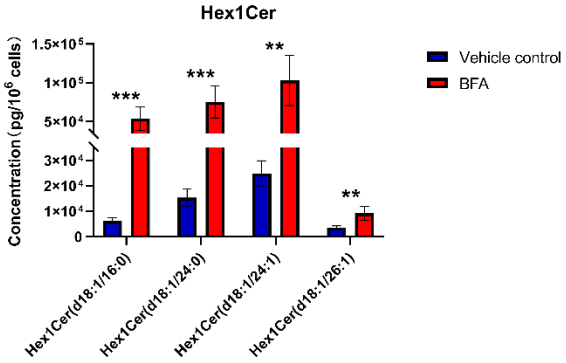
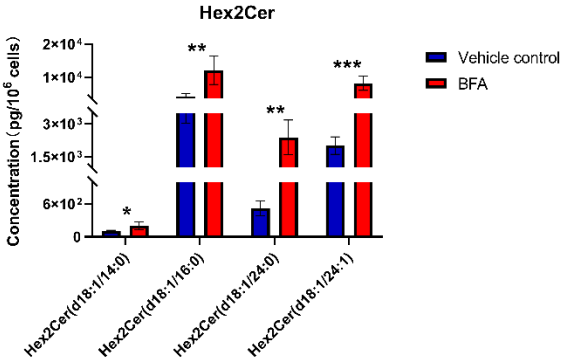
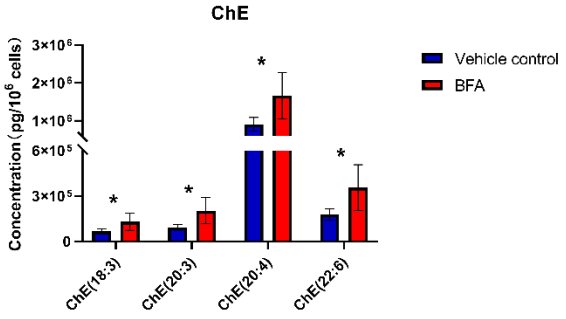


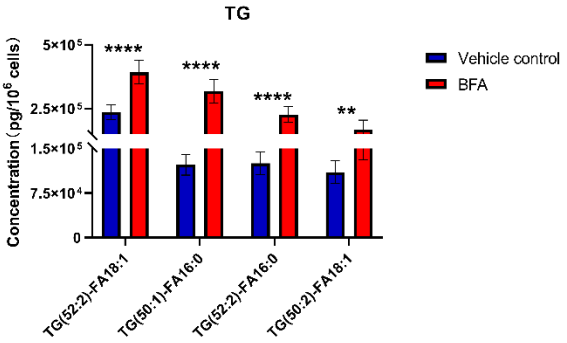
Figure 5. Boxplots of representative LPC, Hex1Cer, Hex2Cer, and FA(24:0) species significantly altered in BFA-treated groups compared to vehicle control groups. LPC and Hex1Cer/Hex2Cer s pecies were significantly increased, while FA(24:0) was significantly decreased. Data are shown as individual values(pg/10^6 cells) with box boundaries representing the interquartile range and wh iskers indicating the 5th-95th percentiles (n = 6 per group). Statistical comparisons were perform ed using Student's t-test with FDR correction. *$p < 0.05$, **$p < 0.01$, ***$p < 0.001$ vs vehicle con trol.











Conclusions

In this study, targeted lipidomics based on UHPLC-QTRAP MS was employed to investigate

the alterations in lipid metabolism induced by Brefeldin A (BFA) in hepatocellular carcinoma (HCC) cells. Our analysis identified profound lipidomic reprogramming, with 481 lipid species significantly altered (FDR < 0.05, $|\log_2 FC| > 0.585$) following 0.25 mg/L BFA treatment. These lipids were categorized into 21 classes across four major categories. Notably, the concentrations of LPC, Hex1Cer, Hex2Cer, ChE, and TG were markedly elevated. Key representative lipid species showing significant increases included LPC(16:0), LPC(17:0), LPC(18:0), LPC(20:0); Hex1Cer(d18:1/16:0), Hex1Cer(d18:1/24:0), Hex1Cer(d18:1/24:1), Hex1Cer(d18:1/26:1); Hex2Cer(d18:1/16:0), Hex2Cer(d18:1/22:0), Hex2Cer(d18:1/24:0), Hex2Cer(d18:1/24:1); ChE(20:3), ChE(20:4), ChE(18:3), ChE(22:6); and TG(48:0)-FA16:0, TG(52:2)-FA16:0, TG(54:4)-FA20:4, TG(56:6)-FA22:6. Conversely, the level of FA(24:0) was significantly decreased. This work systematically delineates the specific lipid metabolic changes triggered by BFA in HCC cells. By quantifying these BFA-induced lipid shifts, our study provides a comprehensive lipid-centric dataset for understanding BFA's cellular effects. The identified lipid species warrant further investigation as candidate markers or potential targets in future mechanistic and functional studies. We acknowledge that the descriptive nature of this study and its limitation to a single cell line call for additional validation experiments to establish the functional significance of these lipid alterations.

Methods

Reagents.

Human hepatocellular carcinoma HepG2 cells were obtained from the Cell Bank of the Chi nese Academy of Sciences (Shanghai, China) (catalog number TCHu 72) .DMEM high-glucose medium was obtained from Gibco (USA). Dimethyl sulfoxide (DMSO) was sourced from Sigm a-Aldrich (USA). Methanol, acetonitrile, isopropanol, water, methyl tert-butyl ether (MTBE), an d ammonium acetate were of HPLC or mass spectrometry grade and were purchased from Therm o Fisher, Sigma-Aldrich, or Aladdin.

Cell Culture and Treatment

Human hepatocellular carcinoma HepG2 cells were cultured in DMEM complete medium supplemented with 10% fetal bovine serum, 100 U/mL penicillin, and 100 U/mL streptomycin, and maintained at 37 °C in a humidified atmosphere containing 5% CO_2. Cells in the logarithmic growth phase were seeded into 100 mm dishes. When cell density reached approximately 80%, the cells were randomly divided into two groups (n = 6 per group): BFA-treated group and vehicle control group. BFA was dissolved in DMSO to prepare a stock solution and subsequently diluted with complete medium to a final concentration of 0.25 mg/L. The vehicle control received an equivalent volume of DMSO (without BFA) in complete medium, ensuring the final DMSO concentration was identical in both groups. Both groups were incubated for 24 h under identical conditions. After treatment, cells were collected for lipid extraction.

Sample Pretreatment and Lipid Extraction.

After slow thawing on ice, an appropriate amount of each sample was mixed with 200 μL methanol by vortexing. Then, 10 μL of internal standard mixture was added, followed by the addition of 800 μL methyl *tert*-butyl ether (MTBE). The mixture was vortexed, sonicated in a chilled water bath for 20 min, and then kept at room temperature for 30 min. Thereafter, 200 μL of mass-spectrometry-grade water was added, and the mixture was vortexed and centrifuged at 14,000 rpm and 4 °C for 15 min. The upper organic phase was collected and dried under a gentle stream of nitrogen. For mass spectrometric analysis, the lipid pellet was reconstituted in 200 μL of 90% isopropanol/acetonitrile solution, thoroughly vortexed, and centrifuged at 14,000 rpm and 4 °C for 15 min. The resulting supernatant was taken for injection and analysis. An aliquot of the cell pellet from each sample was used for total protein quantification by BCA assay, and lipid contents were normalized to total protein (pg/10^6 cells).

Chromatography–Mass Spectrometry Analysis.

Analysis was performed using an ultra-high-performance liquid chromatography system (Shimadzu LC-30AD) coupled to a hybrid triple quadrupole/linear ion trap mass spectrometer (AB Sciex QTRAP® 6500+). Chromatographic conditions: Lipids were separated using a C18 column (Phenomenex, Kinetex C18, 2.1 × 100 mm, 2.6 μm) and an Amino column (Phenomenex, Lun

a NH_2, 2.0 × 100 mm, 3 μm). C18 column: column temperature 45 °C; flow rate 0.35 mL/min; m obile phase A: 70% acetonitrile + 30% water + 5 mM ammonium acetate; mobile phase B: isopr opanol. The gradient elution program was as follows: 0–5.0 min, 20%–60% B; 5.0–13.0 min, 6 0%–100% B; 13.1–17.0 min, 20% B. Amino column: column temperature 40 °C; flow rate 0.4 m L/min; mobile phase A: 2 mM ammonium acetate + 50% methanol + 50% acetonitrile; mobile p hase B: 2 mM ammonium acetate + 50% acetonitrile + 50% water. The gradient elution program was as follows: 0–3.0 min, 3% B; 3.0–13.0 min, 3%–100% B; 13.0–17.0 min, 100% B; 17.1–22. 0 min, 3% B. Throughout the analysis, samples were kept in the autosampler at 10 °C. To minimi ze the influence of instrumental signal fluctuations, samples were analyzed in a random order. A pooled quality control (QC) sample was prepared and injected periodically throughout the run to evaluate system stability and repeatability; lipid species with a coefficient of variation (CV) < 3 0% in QC samples were retained for further analysis. Mass spectrometric conditions: Detection was carried out in both electrospray ionization (ESI) positive-ion and negative-ion modes. ESI so urce parameters were set as follows: source temperature 400 °C; ion source gas 1 (GS1) 50; ion s ource gas 2 (GS2) 55; curtain gas (CUR) 35; ion spray voltage (IS) +3000 V in positive mode an d –2500 V in negative mode. Analysis was performed in multiple reaction monitoring (MRM) m ode. Quantification was achieved using isotope-labeled internal standards (one per lipid class); th e concentration of each lipid was calculated by comparing the peak area ratio of the analyte to its corresponding internal standard against a multi-point calibration curve prepared from authentic l ipid standards.

Data Analysis

Lipid identification and quantification were accomplished via a targeted approach, combinin g multiple reaction monitoring (MRM) with isotope-labeled internal standards to achieve high sp ecificity and accuracy. Quantification was achieved using isotope-labeled internal standards (one per lipid class); the concentration of each lipid was calculated by comparing the peak area ratio o f the analyte to its corresponding internal standard against a multi-point calibration curve prepare

d from authentic lipid standards. Peak extraction and quantitative analysis of MRM data were per formed using Sciex OS software.

For quality control, lipid species detected in QC samples with a coefficient of variation (C V) < 30% were considered reproducible and retained for further analysis.

For statistical analysis, unsupervised pattern recognition (principal component analysis, PC A) was first employed to provide an overview of the data structure and detect any inherent cluste ring or outliers. Subsequently, supervised pattern recognition (partial least squares-discriminant a nalysis, PLS-DA) was applied to maximize the separation between groups and to identify the lipi d species contributing most to group discrimination. The variable importance in projection (VIP) score from the PLS-DA model (VIP > 1.0) was used to select potential candidate lipids. For univ ariate analysis, two-sided Student's t-test was applied. To control the false discovery rate (FDR) i n multiple comparisons, the Benjamini-Hochberg procedure was used. Lipids meeting both criter ia (VIP > 1.0 and FDR < 0.05) were considered significantly altered.

Funding

This work was supported by the National Natural Science Foundation of China (NSFC 3097 2445), the Natural Science Foundation of Shanxi Province of China (202203021211231), and the Shanxi Province Higher Education "Billion Project" Science and Technology Guidance Project.

Clinical trial number

not applicable.

Ethics, Consent to Participate, and Consent to Publish declarations

not applicable.

Declarations

Ethics approval and consent to participate

Not applicable. This study did not involve human participants, human data, or human tissue.

Consent for publication

Not applicable. This manuscript does not contain any individual person's data in any form.

Data availability statement

The datasets generated and/or analyzed during the current study are available from the corre sponding author upon reasonable request.

Competing interests

The authors declare no competing interests.

REFERENCES

1. Sung, H.; Ferlay, J.; Siegel, R. L.; Laversanne, M.; Soerjomataram, I.; Jemal, A.; Bray, F. Global Cancer Statistics 2020: GLOBOCAN Estimates of Incidence and Mortality Worldwide for 36 Cancers in 185 Countries. *CA: A Cancer Journal for Clinicians* **2021**, *71* (3), 209-249. DOI: 10.3322/caac.21660.

2. Zheng, R.; Zhang, S.; Zeng, H.; Wang, S.; Sun, K.; Chen, R.; Li, L.; Wei, W.; He, J. Cancer incidence and mortality in China, 2016. *Journal of the National Cancer Center* **2022**, *2* (1), 1-9. DOI: 10.1016/j.jncc.2022.02.002.

3. Peyroche, A.; Antonny, B.; Robineau, S.; Acker, J.; Cherfils, J.; Jackson, C. L. Brefeldin A acts to stabilize an abortive ARF-GDP-Sec7 domain protein complex: involvement of specific residues of the Sec7 domain. . *Mol Cell.* **1999**, 3(3):275-285. DOI: 10.1016/s1097-2765(00)80455-4.

4. Klausner, R. D.; Donaldson, J. G.; Lippincott-Schwartz, J. Brefeldin A: insights into the control of membrane traffic and organelle structure. *The Journal of cell biology* **1992**, *116* (5), 1071-1080. DOI: 10.1083/jcb.116.5.1071.

5. Citterio, C.; Vichi, A.; Pacheco-Rodriguez, G.; Aponte, A. M.; Moss, J.; Vaughan, M. Unfolded protein response and cell death after depletion of brefeldin A-inhibited guanine nucleotide-exchange protein GBF1. . *Proc Natl Acad Sci USA.* **2008**, 105(108):2877-2882. DOI: 10.1073/pnas.0712224105.

6. Che, L.; Chi, W.; Qiao, Y.; Zhang, J.; Song, X.; Liu, Y.; Li, L.; Jia, J.; Pilo, M. G.; Wang, J.; et al. Cholesterol biosynthesis supports the growth of hepatocarcinoma lesions depleted of fatty acid synthase in mice and humans. *Gut* **2020**, *69* (1), 177-186. DOI: 10.1136/gutjnl-2018-317581.

7. Sangineto, M.; Villani, R.; Cavallone, F.; Romano, A.; Loizzi, D.; Serviddio, G. Lipid Metabolism in Development and Progression of Hepatocellular Carcinoma. *Cancers* **2020**, *12* (6). DOI: 10.3390/cancers12061419.

8. Yagin, F. H.; Colak, C.; Al-Hashem, F.; Alzakari, S. A.; Alhussan, A. A.; Aghaei, M. Identification of a Novel Lipidomic Biomarker for Hepatocyte Carcinoma Diagnosis: Advanced Boosting Machine Learning Techniques Integrated with Explainable Artificial Intelligence. *Metabolites* **2025**, *15* (11). DOI: 10.3390/metabo15110716.

9. Xu, C.; Song, D.; Holck, A. L.; Zhou, Y.; Liu, R. Identifying Lipid Metabolites Influenced by Oleic Acid Administration Using High-Performance Liquid Chromatography–Mass Spectrometry-Based Lipidomics. *ACS Omega* **2020**, *5* (20), 11314-11323. DOI: 10.1021/acsomega.9b04402.

10. Migni, A.; Bartolini, D.; Marcantonini, G.; Sardella, R.; Rende, M.; Tognoloni, A.; Ceccarini, M. R.; Galli, F. Multivariate Data Analysis Methods and Their Application in Lipidomics: A Gentle Comment on Appropriateness and Reliability Criteria. *Journal of Pineal Research* **2025**, *77* (4). DOI: 10.1111/jpi.70068.

11. Chappel, J. R.; Kirkwood-Donelson, K. I.; Reif, D. M.; Baker, E. S. From big data to big insights: statistical and bioinformatic approaches for exploring the lipidome. *Analytical and Bioanalytical Chemistry* **2023**, *416* (9),

2189-2202. DOI: 10.1007/s00216-023-04991-2.
12. Zhou, M.; Sun, W.; Gao, Y.; Jiang, B.; Sun, T.; Xu, R.; Zhang, X.; Wang, Q.; Xuan, Q.; Ma, S. Metabolomic profiling reveals interindividual metabolic variability and its association with cardiovascular-kidney-metabolic syndrome risk. *Cardiovascular Diabetology* **2025**, *24* (1). DOI: 10.1186/s12933-025-02881-8.
13. Jokesch, P.; Oskolkova, O.; Fedorova, M.; Gesslbauer, B.; Bochkov, V. Contribution of individual phospholipase A2 enzymes to the cleavage of oxidized phospholipids in human blood plasma. *Journal of Lipid Research* **2025**, *66* (2). DOI: 10.1016/j.jlr.2025.100742.
14. Lin, P.; Ye, R. D. The Lysophospholipid Receptor G2A Activates a Specific Combination of G Proteins and Promotes Apoptosis. *Journal of Biological Chemistry* **2003**, *278* (16), 14379-14386. DOI: 10.1074/jbc.M209101200.
15. Mei-Chi Chang, J.-J. L., Yi-Jane Chen, Wen Liou, Wei-Ling Huang, Chiu-Po Chan , Szu-I Lin, Li-Deh Lin , Eric Jein, Chi-Chia Huang and Jiiang-Huei Jeng. Lysophosphatidylcholine induces cytotoxicity/apoptosis and IL-8 production of human endothelial cells: Related mechanisms. *Oncotarget* **2017**, 8(63):106177-106189. DOI: 10.18632/oncotarget.22420.
16. Chen, H.; Ma, J.; Liu, J.; Dou, L.; Shen, T.; Zuo, H.; Xu, F.; Zhao, L.; Tang, W.; Man, Y.; et al. Lysophosphatidylcholine disrupts cell adhesion and induces anoikis in hepatocytes. *FEBS Letters* **2022**, *596* (4), 510-525. DOI: 10.1002/1873-3468.14291.
17. Lebeaupin, C.; Vallée, D.; Hazari, Y.; Hetz, C.; Chevet, E.; Bailly-Maitre, B. Endoplasmic reticulum stress signalling and the pathogenesis of non-alcoholic fatty liver disease. *Journal of Hepatology* **2018**, *69* (4), 927-947. DOI: 10.1016/j.jhep.2018.06.008.
18. Maiers, J.; Malhi, H. Endoplasmic Reticulum Stress in Metabolic Liver Diseases and Hepatic Fibrosis. *Seminars in Liver Disease* **2019**, *39* (02), 235-248. DOI: 10.1055/s-0039-1681032.
19. Jan Willem Kok, T. B., Catalin M. Filipeanu, Adriaan Nelemans, Gustavo Egea, and Dick Hoekstra. PDMP Blocks Brefeldin A–induced Retrograde Membrane Transport from Golgi to ER: Evidence for Involvement of Calcium Homeostasis and Dissociation from Sphingolipid Metabolism. *J Cell Biol* **1998**, 142(141):125-138. DOI: 10.1083/jcb.142.1.25.
20. Spinedi, A. Brefeldin A Limits N-Hexanoylsphingosine-Induced Accumulation of Natural Ceramide via the Salvage Pathway by Enhancing Glucosylation. *Lipids* **2013**, *49* (2), 207-210. DOI: 10.1007/s11745-013-3858-3.
21. Straus, A. J.; Mavodza, G.; Senkal, C. E. Glycosylation of ceramide synthase 6 is required for its activity. *Journal of Lipid Research* **2025**, *66* (1). DOI: 10.1016/j.jlr.2024.100715.
22. Hayashi, Y.; Tanikawa, T. Analysis of the Effects of Brefeldin A on Deuterium-Labeled Sphinganine Metabolism Using Liquid Chromatography–Tandem Mass Spectrometry. *Biological and Pharmaceutical Bulletin* **2024**, *47* (12), 2173-2181. DOI: 10.1248/bpb.b24-00292.
23. Garcia-Ruiz, C.; Morales, A.; Fernández-Checa, J. C. Glycosphingolipids and cell death: one aim, many ways. *Apoptosis* **2015**, *20* (5), 607-620. DOI: 10.1007/s10495-015-1092-6.
24. Sano, R.; Annunziata, I.; Patterson, A.; Moshiach, S.; Gomero, E.; Opferman, J.; Forte, M.; d'Azzo, A. GM1-Ganglioside Accumulation at the Mitochondria-Associated ER Membranes Links ER Stress to Ca2+-Dependent Mitochondrial Apoptosis. *Molecular Cell* **2009**, *36* (3), 500-511. DOI: 10.1016/j.molcel.2009.10.021.
25. García-Ruiz, C.; Colell, A.; París, R.; Fernández-Checa, J. C. Direct interaction of GD3 ganglioside with mitochondria generates reactive oxygen species followed by mitochondrial permeability transition,

cytochrome c release, and caspase activation. *The FASEB Journal* **2000**, *14* (7), 847-858. DOI: 10.1096/fasebj.14.7.847.
26. Mesicek, J.; Lee, H.; Feldman, T.; Jiang, X.; Skobeleva, A.; Berdyshev, E. V.; Haimovitz-Friedman, A.; Fuks, Z.; Kolesnick, R. Ceramide synthases 2, 5, and 6 confer distinct roles in radiation-induced apoptosis in HeLa cells. *Cellular Signalling* **2010**, *22* (9), 1300-1307. DOI: 10.1016/j.cellsig.2010.04.006.
27. Silva, L. C.; Ben David, O.; Pewzner-Jung, Y.; Laviad, E. L.; Stiban, J.; Bandyopadhyay, S.; Merrill, A. H.; Prieto, M.; Futerman, A. H. Ablation of ceramide synthase 2 strongly affects biophysical properties of membranes. *Journal of Lipid Research* **2012**, *53* (3), 430-436. DOI: 10.1194/jlr.M022715.
28. Zelnik, I. D.; Volpert, G.; Viiri, L. E.; Kauhanen, D.; Arazi, T.; Aalto-Setälä, K.; Laaksonen, R.; Futerman, A. H. Different rates of flux through the biosynthetic pathway for long-chain versus very-long-chain sphingolipids. *Journal of Lipid Research* **2020**, *61* (10), 1341-1346. DOI: 10.1194/jlr.RA120000984.
29. Stein; b, Y. D.; Hollander, G.; Ben-Naim, M.; Stein, Y. Dissimilar effects of Brefeldin A on cholesteryl ester and triacylglycerol metabolism in CaCo2 and HepG2 cells as compared to peritoneal macrophages. *Journal of Lipid Research* **1991**, *33(32)*, 217-226. DOI: 10.1016/0005-2760(92)90151-k.
30. Hasumi, K.; Naganuma, S.; Koshizawa, J.; Mogi, H.; Endo, A. Stimulation of acyl-CoA:cholesterol acyltransferase activity by brefeldin A in macrophage J774 cells. *Biochim Biophys Acta* **1993**, *1167* (2), 155-158. DOI: 10.1016/0005-2760(93)90156-4 From NLM.
31. Gawlak-Socka, S.; Kowalczyk, E.; Wiktorowska-Owczarek, A. Unfolded Protein Response at the Crossroads: Integrating Endoplasmic Reticulum Stress with Cellular Stress Networks. *International Journal of Molecular Sciences* **2026**, *27* (4). DOI: 10.3390/ijms27041986.
32. Aronis, A.; Madar, Z.; Tirosh, O. Mechanism underlying oxidative stress-mediated lipotoxicity: Exposure of J774.2 macrophages to triacylglycerols facilitates mitochondrial reactive oxygen species production and cellular necrosis. *Free Radical Biology and Medicine* **2005**, *38* (9), 1221-1230. DOI: 10.1016/j.freeradbiomed.2005.01.015.
33. Smolková, K.; Gotvaldová, K. Fatty Acid Trafficking Between Lipid Droplets and Mitochondria: An Emerging Perspective. *International Journal of Biological Sciences* **2025**, *21* (5), 1863-1873. DOI: 10.7150/ijbs.105361.

Supplementary Files

This is a list of supplementary files associated with this preprint. Click to download.

- Table1.xlsx